Received August 20, 2021, accepted September 17, 2021, date of publication September 20, 2021,
date of current version September 30, 2021.

Digital Object Identifier 10.1109/ACCESS.2021.3114212

Use of a 3-D Wireless Power Transfer Technique as a Method for Capsule Localization

SADEQUE REZA KHAN[1], SRINJOY MITRA[1], (Senior Member, IEEE), AND MARC P. Y. DESMULLIEZ[2], (Senior Member, IEEE)

[1]School of Engineering, Institute of Integrated Micro and Nano Systems, The University of Edinburgh, Edinburgh EH9 3FF, U.K.
[2]School of Engineering and Physical Sciences, Institute of Sensors, Signals, and Systems, Heriot-Watt University, Edinburgh EH14 4AS, U.K.

Corresponding author: Sadeque Reza Khan (sadeque.khan@ed.ac.uk)

This work was supported by U.K. Engineering and Physical Sciences Research Council (EPSRC) through the Programme Grant entitled Sonopill under Grant EP/K034537/2 and the Platform Grant 4-MD under Grant EP/P027415/1. The work of Sadeque Reza Khan was supported by Heriot-Watt University through the International Doctoral Training Account (DTA).

ABSTRACT Capsule endoscopy has been heralded as a technological milestone in the diagnosis and therapeutics of gastrointestinal (GI) pathologies. The location and position of the capsule within the GI tract are important information for subsequent surgical intervention or local drug delivery. Accurate information of capsule location is therefore required during endoscopy. Although radio frequency (RF)-based, magnetic tracking and video localization have been investigated in the past, the complexity of those systems and potential inaccuracy in the localization data necessitate the scope for further research. This article proposes the dual use of a wireless power transfer (WPT) configuration as a method to enable the determination of the location of an endoscopic capsule. Measurements conducted on a homogeneous agar-based liquid phantom predict a maximum error of 12% between the calculated and measured trajectories of the capsule in a working volume of 100 mm × 100 mm × 100 mm.

INDEX TERMS 3-D receiver, capsule endoscopy, localization technique, liquid phantom, wireless power transfer.

I. INTRODUCTION

Real-time localization (lower intestine, duodenum, etc. and location within) of an endoscopic capsule within the gastrointestinal (GI) tract has been the subject of many research studies over recent years [1]–[3]. This information is important for several reasons. (1) The exact placement of the pathologies within the GI tract is provided by the capsule for subsequent surgical intervention; (2) the frame rate of the camera within the capsule can be adjusted for optimal video transmission of the pathology, enabling power savings for battery-powered capsules, (3) an insertion path for future biomedical devices can be determined to avoid repetitive attempts of invasive endoscopy; (4) the location can be used to reconstruct the travel path of the capsule inside the GI tract which can be helpful for micro-robotic surgeries or the creation of a ''gut-atlas'', for example.

Accurate localization techniques include the use of radio frequency (RF) methods [2], magnetic tracking [4], video localization [5], medical imaging [6], ultrasound [7], X-ray [8], gamma ray [9] and positron emission tomography (PET) [10]. The common RF-based localization approach uses a two-step estimation process to determine the location of the capsule. The first step is based on the use of multiple sensors and antennas mounted on the human body that measure one or more signal parameters related to the location of the transmitter installed inside the capsule, such as received-signal-strength (RSS), time-of-arrival (TOA), direction-of-arrival (DOA) or angle-of arrival (AOA) [11]. In the second step, statistical algorithms process these parameters to estimate the best location of the capsule.

RSS is a key signal property which can be acquired without any hardware overhead [1]. A receiver sensor measures the strength of the signal recovered to estimate the distance of the capsule from the transmitter [2]. One of the first RSS-based localization systems used eight external antennas to measure the RSS of data transmitted from a capsule [12]. This technique was utilized for the M2A capsule (precursor of PillCam) commercialized by Given Imaging Ltd. Generally, a signal propagation model is used to relate the RSS to

The associate editor coordinating the review of this manuscript and approving it for publication was Anandakumar Haldorai.

the distance between the internal TX and the RX antennas mounted on the body [3], [12], [13]. A trilateration algorithm is applied to the distance data to calculate the coordinates of the capsule. In [14], a look-up table-based approach is adopted instead of a propagation path model to estimate the location of the capsule. The proposed algorithm compares the measured RSS data with the off-line measurement data of the look-up table and provides the predicted position of the capsule. A more accurate propagation model that includes the antenna orientation and tissue absorption along with the distance data is presented in [15]. In [16], the antenna radiation pattern is utilized to improve the accuracy of the localization. The detailed analysis of radio wave propagation in different human tissues is carried out by calculating the path loss parameters at various frequencies. Further, the path loss is compensated using both the distance and azimuth data in the GI parts of the human body. Despite all these improvements, RSS suffers from multi-path effects, such as reflection, refraction, diffraction and shadowing due to the complex and unpredictable environmental conditions inside the human body. Furthermore, ToA utilizes precision clock to measure distance with proper synchronization [17], AoA calculates the distance by using an array of directional antennas and estimation algorithm [18], and RFID-based technique uses cubic antenna array to detect tag location [19]–[21].

This article proposes a wireless power transfer (WPT)-based configuration which also acts as a localization system. A WPT method with 3-D configuration for the receiver (RX) coil was presented in [22] to enable good power transfer efficiency that accommodates time-varying locations of the capsule with the GI tract. This work utilizes the architecture of the 3-D cross-type RX coil and demonstrates, using analytical, simulated and measurement results, that the RX output power variation due to the varying magnetic field generated by a multi-transmitter (TX) system, can also be exploited to estimate the location of the capsule within the GI tract where [22] only describes the WPT technique. The configuration is similar to the RSS method with the difference that the power is transmitted from outside the body onto the capsule. The location is then predicted based on the amount of power received by the three coils of the receivers inside the capsule. The measurement was conducted on a homogeneous agar-based liquid phantom. The simulated RX output power values are considered as the reference data and are stored in a look-up table. Five sample values are measured and compared with the reference data to assess the accuracy of the proposed WPT-based localization technique. A maximum percentage of error of 12% is achieved which translates to a ±13 mm inaccuracy regarding the location of the capsule within a 100 mm×100 mm×100 mm volume inside a mannequin filled with liquid phantom.

II. WPT THEORY

In [22], a 3-D WPT technique is presented for capsule endoscopy (CE) where a miniaturized 3-D cross type RX coil can receive power from any direction from two flexible TX coils. The schematic of the 3-D configuration for the WPT RX system is reproduced in Fig. 1 for one TX coil.

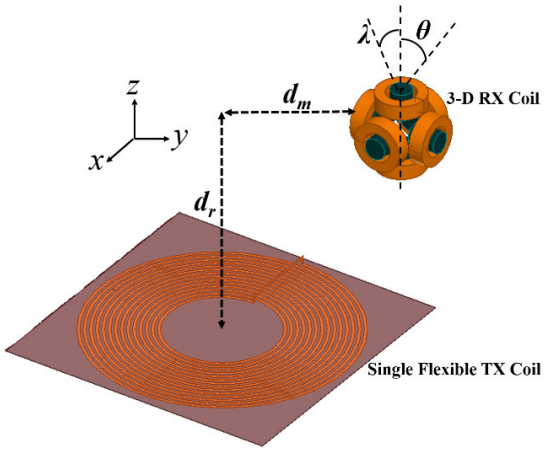

FIGURE 1. Schematic view of 3-D WPT method reproduced from [22]. 3 ferrite rods are inserted inside the 3 mutually perpendicular coils.

The mutual inductance between TX and RX coils for a separation distance, d_r, between the two loops, translational misalignment of d_m, roll and pitch rotational angle of θ and λ, respectively, can be derived as [23]:

$$M = \frac{\mu\pi R_{C1}^2 R_{C2}^2 \cos\theta\cos\lambda}{2\left(R_{C1}^2 + R_{C2}^2 + d_r^2 + d_m^2\right)^{\frac{3}{2}}} \times \begin{bmatrix} 1 + \frac{15}{64}\left(\gamma_a^2 + 4\gamma_b^2\right) + \frac{15}{64}\left(\gamma_a^2 + 4\gamma_c^2\right) \\ \cos^2\theta\cos^2\lambda + \frac{15}{8}\gamma_d^2\left(\sin\theta\cos\lambda\sin\lambda\cos\theta\right) \\ -\frac{15}{8}\gamma_c\gamma_d\cos\theta\cos\lambda\left(\sin\theta\cos\lambda + \sin\lambda\cos\theta\right) \\ -\frac{3}{2}\left(\delta_a - \delta_b\left(\tan\theta + \tan\lambda\right)\right) \end{bmatrix} \quad (1)$$

where μ is the permeability of the medium surrounding the coils, and R_{C1}, R_{C2} are the radii of the TX coils C1 and C2, respectively. In (1), the parameters γ_a, γ_b, γ_c and γ_d are smaller than unity and defined in [23] alongside δ_a and δ_b as:

$$\gamma_a = \frac{2R_{C1}R_{C2}}{R_{C1}^2 + R_{C2}^2 + d_r^2 + d_m^2} \quad (2)$$

$$\gamma_b = \frac{2R_{C1}d_2}{R_{C1}^2 + R_{C2}^2 + d_r^2 + d_m^2} \quad (3)$$

$$\gamma_c = \frac{2R_{C2}d_2}{R_{C1}^2 + R_{C2}^2 + d_r^2 + d_m^2} \quad (4)$$

$$\gamma_d = \frac{2R_{C2}d_r}{R_{C1}^2 + R_{C2}^2 + d_r^2 + d_m^2} \quad (5)$$

$$\delta_a = \frac{d_2^2}{R_{C1}^2 + R_{C2}^2 + d_r^2 + d_m^2} \quad (6)$$

$$\delta_b = \frac{d_2 d_r}{R_{C1}^2 + R_{C2}^2 + d_r^2 + d_m^2} \quad (7)$$

The total mutual inductance, M_{total}, can be defined as [15]–[17]:

$$M_{total} = \sum_{i=1}^{T_{C1}} \sum_{j=1}^{T_{C2}} \sum_{k=1}^{L_{C1}} \sum_{l=1}^{L_{C2}} M \begin{pmatrix} R_{C1:k}, R_{C2:l}, \\ d_{r(i,j)}, d_m, \theta, \lambda \end{pmatrix} \times \left[2 - \frac{R_F^2}{R^2} \left(1 - \frac{\mu_F}{1 + D_c(\mu_F - 1)} \right) \right] \quad (8)$$

where coil C1 contains T_{C1} layers and L_{C1} loops, and coils C2 contains T_{C2} layers and L_{C2} loops. R, R_F, μ_F and D_c are the radii of the receiver coil and the ferrite rod, the relative intrinsic permeability of the ferrite material and the demagnetizing factor [22], [24], respectively.

The power transfer efficiency (PTE) of the two TX WPT system, η_{RX}, can be defined using coupled mode theory as the ratio between the total power delivered to the system from the source, P_S, and P_L, the power delivered to the load via the receiver RX [22].

$$\eta_{RX} = \frac{P_L}{P_S} = \frac{1}{2 + \frac{Q_L}{Q_{RX}} \left[2 + \frac{1}{FOMD^2} \left(1 + \frac{Q_{RX}}{Q_L} \right)^2 \right]} \quad (9)$$

where Q_{RX} and Q_L ($=2\pi f L_{RX}/R_L$) are the quality factor (Q-factor) of the RX coil and load, respectively [25]–[27]. Further, f, L_{RX} and R_L are the operating frequency, self-inductance of the RX coil and load resistor, respectively. According to the energy conservation theory, $P_S = P_{TX1} + P_{TX2} + P_{RX} + P_L$, where P_{TX1}, P_{TX2} and P_{RX} are the powers of the TX1, TX2 and RX coils, respectively [28]–[30]. The distance-dependent figure of merit ($FOMD$) is defined as [22]:

$$FOM = \sqrt{k_{TX1,RX}^2 Q_{TX1} Q_{RX} + k_{TX2,RX}^2 Q_{TX2} Q_{RX}} \quad (10)$$

where Q_{TX1} and Q_{TX2} are Q-factor of the TX1 and TX2 coils. The term k_{ij} is the distance-dependent coupling coefficient between coil i and j. The total PTE can then be written as [22]:

$$\eta_{total} = \eta_{RX}\,(x - axis) + \eta_{RX}\,(y - axis) + \eta_{RX}\,(z - axis) \quad (11)$$

Using (9) and (11) it is possible to calculate the approximated received power for different d_r and d_m which can help predict the location of the RX coil inside a capsule.

III. PROPOSED LOCALIZATION TECHNIQUE

Figure 2 illustrates, as a proof-of-principle of this concept, the configuration of the proposed WPT-based localization technique. Two orthogonal printed spiral flexible TX coils of 200 mm diameter are used to transmit power to an 8 mm diameter RX coil embedded into an endoscopic capsule. The RX receiver system is composed of three wire-wound coils placed orthogonally to each other [22].

The proposed technique is an alternative configuration to the RSS-based method where the localization is estimated by measuring the signal strength transmitted to the capsule with the RX placed inside the capsule this time. In this system,

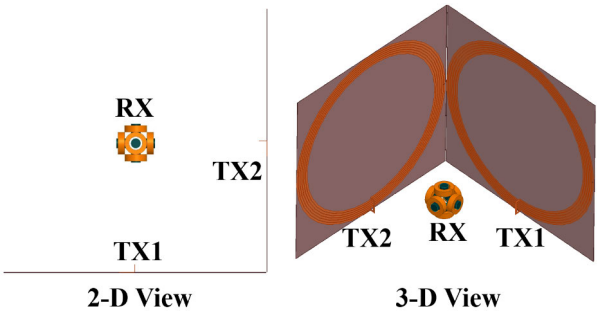

FIGURE 2. Proposed WPT-based localization and positioning technique. Left: top view; right: perspective view.

the three receiver coils record different received power intensities, which, by looking at a look-up table and accounting for the history of the position of the capsule, provide the location for the capsule. Different RX output power intensities are measured as the capsule is displaced with respect to the TX coils. The mapping of the intensities for each receiver coil with its position makes it possible to estimate the orientation of the capsule within the magnetic field configuration defined by the two transmitter coils.

The magnetic field distribution between the TX and RX coils was simulated for 3 positions of the receiver (25 mm, 100 mm and 175 mm distance from both TX coils), an example of which is given in Fig. 3.

The simulation was conducted using the 3D electromagnetic (EM) field solver ANSYS MAXWELL 3D^{TM}. The input power per TX coil is set as 5 W (total input power is 10 W) for the simulation and measurement results. The strength of the magnetic field is high near the TX coils leading to the RX recording a high power. As expected, the power received by the 3-D coil decreases as the RX is positioned further away from the TX coils. Therefore, the received power can be utilized to estimate how far the CE inside GI tract is away from the coils.

IV. EXPERIMENTAL SETUP FOR THE LOCALIZATION OF THE CAPSULE

Figure 4 shows the capsule localization measurement setup with the liquid phantom poured into a hollow polystyrene-based half-mannequin [22]. The TX coils are positioned orthogonally, as previously shown in Fig. 2. Only the presumed location of GI tract is filled with the prepared phantom. The TX coils have been manufactured in flexible PCB that can be either printed onto or inserted into a patient's wearable jacket in future applications. The influence of the bending of the TX coil on the power transfer efficiency is minimum as demonstrated in [22].

The specific absorption rate (SAR) simulation results of two 200 mm diameter TX coils around a human body is presented in Fig. 5 using the ANSYS HFSS human model. SAR is an important parameter used to quantify the maximum possible exposure of any biological tissue with respect to radio frequency (RF) radiation. At a frequency of 5 MHz and for 5 W of input power for each of the TX, the simulated

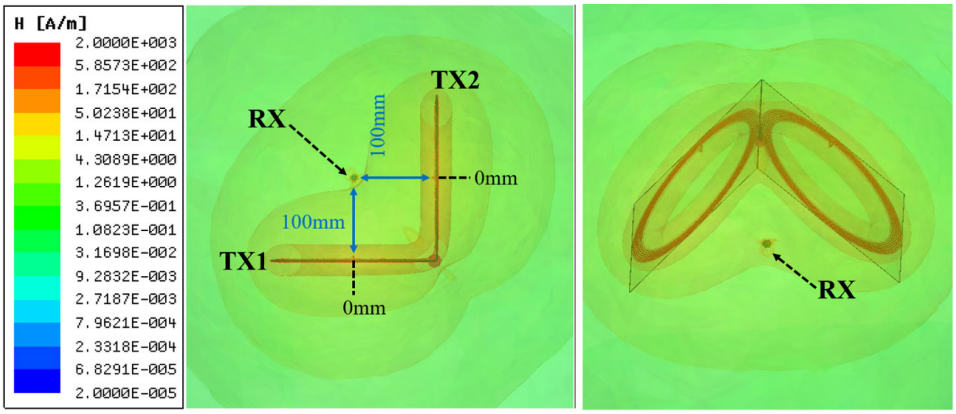

FIGURE 3. Example of magnetic field distribution of the proposed localization and positioning technique with 3-D RX placed at middle distance of the TX coils. The RX coil is 100 mm away from TX1 and TX2 and aligned with the centers of the two coils.

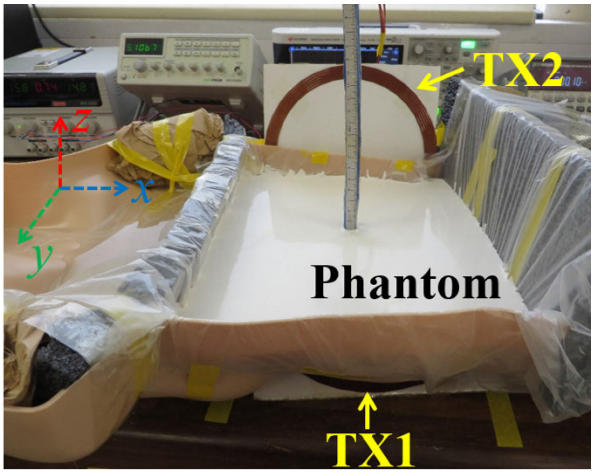

FIGURE 4. Localization measurement in liquid phantom using 3-D cross-type RX. The outer diameter of TX1 and TX2 is 200 mm.

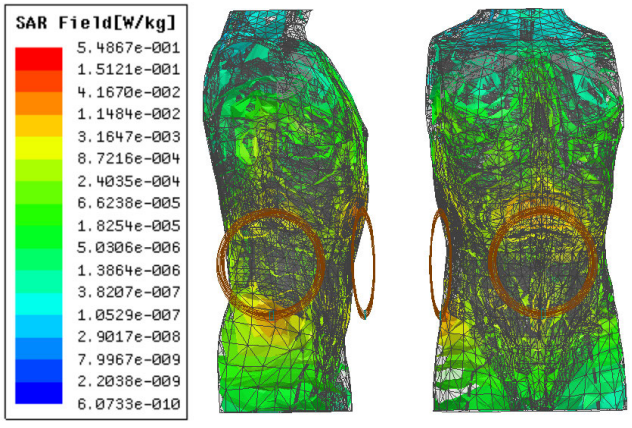

FIGURE 5. Position of TX coils in human body including SAR measurement.

SAR value of 0.55 W/kg is lower than the IEEE standard of 2 W/Kg for 10 g of human tissue [31]. The proposed system is therefore safe to use on a human body.

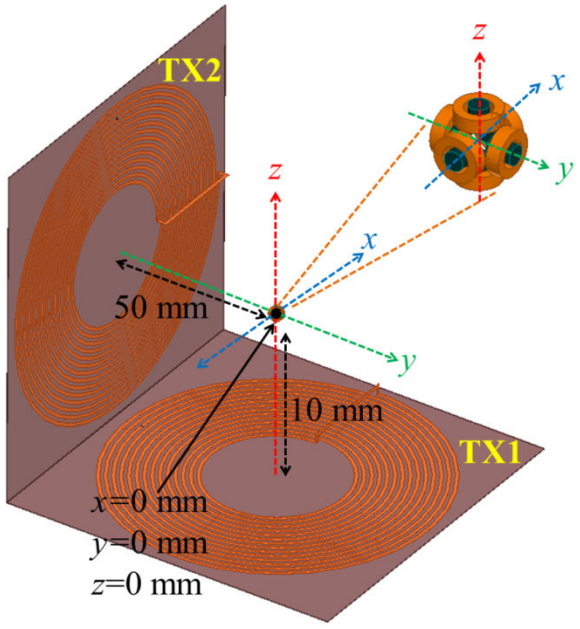

FIGURE 6. Cartesian coordinate system used for the localization measurement.

Figure 6 shows the schematic setup for the proposed WPT-based localization technique with the origin of the x, y, z orthogonal reference system taken as the solid black circle. On the x-axis, the initial position of the capsule, $x = 0$ mm, is assumed to be at the intersection of the rotational axes of both TX1 and TX2. As the TX coils are placed outside the mannequin, the origin of the y-axis is 50 mm away from the TX2 coil due to the shape of the mannequin. Similarly, the origin of the z-axis is 10 mm away from the TX1 coil due to the thickness and curvature of the mannequin.

A. PREPARATION OF THE PHANTOM

The composition of the highly hydrous gel phantom is listed in Table 1. Relative dielectric permittivity and conductivity are tuned by adjusting the relative proportion of the

TABLE 1. Composition of the prepared phantom.

Materials	Weight (g)	Ratio with respect to PW	Functions
Purified water (PW)	26	1	Primary material
Polyethylene Powder	2.6	0.1	Relative permittivity
NaCl	0.3016	0.0116	Conductivity
Agar	0.8	0.0309	Forming
Hydroxyethyl Cellulose	0.65	0.025	Thickener
Dehydroacetic acid sodium salt	0.026	0.001	Antiseptic

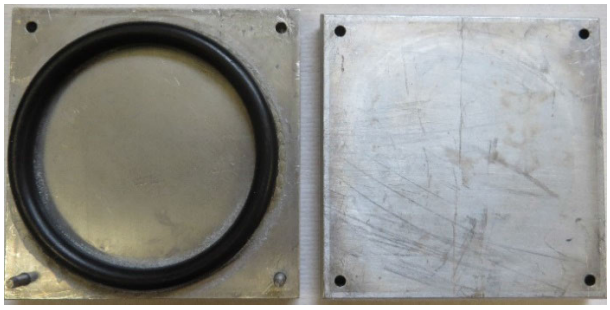

FIGURE 7. Parallel plate capacitance test fixture.

polyethylene powder and NaCl, respectively. Agar is employed for forming, hydroxyethyl cellulose is used as a thickener, and dehydroacetic acid sodium salt is an antiseptic. Purified water (PW) is the main material to prepare the phantom.

The relative permittivity and conductivity of the phantom are measured using the technique derived from [32]. The measurement fixture for the prepared phantom consists of two square aluminum plates of width $a = 8$ cm, as shown in Fig. 7. A polytetrafluoroethylene (PTFE) solid torus of $r = 3.5$ cm radius is employed to prevent misalignment and to hold the liquid phantom between the metal plates. As the extremities of the square plates overhang the solid torus, the total capacitance, C_{tot}, can be written as the sum of the two resulting parallel capacitances: one defined by the liquid phantom, the other by the overhang in air. The relative permittivity of the PTFE torus is neglected due to its small cross-section area.

The relative permittivity of the phantom, ε_1, can be calculated as

$$\varepsilon_1 = 1 + \left(\frac{dC_{tot}}{\varepsilon_o a^2} - 1\right)\frac{a^2}{\pi r^2} \tag{12}$$

where ε_0 and d are the dielectric permittivity of vacuum and distance between the parallel plates, respectively. The conductivity is defined as

$$\sigma = \frac{d}{R_{res}A} \tag{13}$$

where R_{res} is the measured resistance of the parallel plates and A is the disc area defined by the phantom.

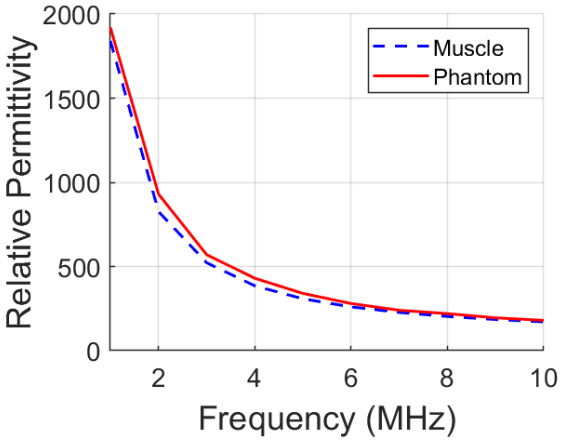

FIGURE 8. Relative dielectric permittivity of the phantom.

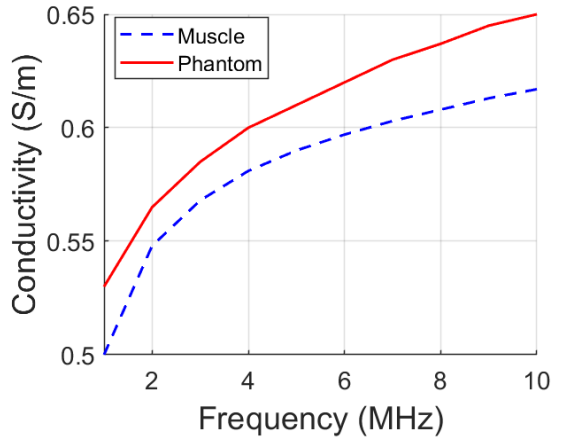

FIGURE 9. Electrical conductivity of the phantom.

The total capacitance and resistance have been measured using the impedance analyzer HP4192A. Fig. 8 and Fig. 9 show the variation from 1 to 10 MHz of the relative dielectric permittivity (left) and conductivity (right). The prepared phantom has a maximum error of 8% and 5% at 5 MHz and 10 MHz, respectively for the relative permittivity, and 3% and 6% at 5 MHz and 10 MHz, for the electrical conductivity compared to values obtained for real human muscle [33].

B. MEASUREMENT RESULTS

1) MEASUREMENT IN AIR

Measurements were conducted first in air to ascertain that the values of the received powers conform to the simulated results obtained from the electromagnetic (EM)-solver ANSYS MAXWELL. Analytical power values obtained from Equations (1) to (11) were also calculated using MATLAB R2019a. Figures 10 to 15 present the analytical, simulated and experimental results of the power calculated or measured for the y-coil (horizontal coil, green arrow) and z-coil (vertical coil, red arrow) of the 3D-RX of Figure 6 as the coil is moved diagonally from the origin on the x-z plane defined by $y = 0$. The x-coil of 3-D RX is positioned orthogonally

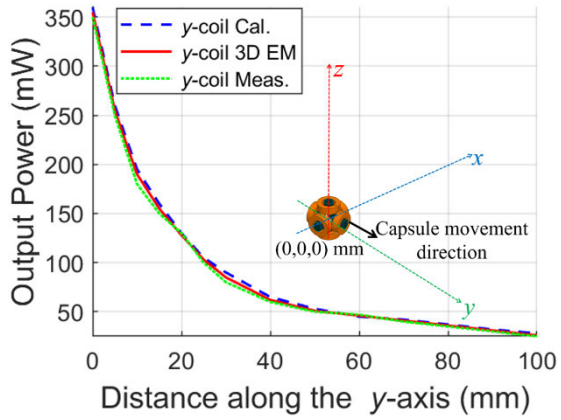

FIGURE 10. Output power variation obtained by the *y*-coil with respect to distance along the *y*-axis while $x = 0$ mm and $z = 0$ mm.

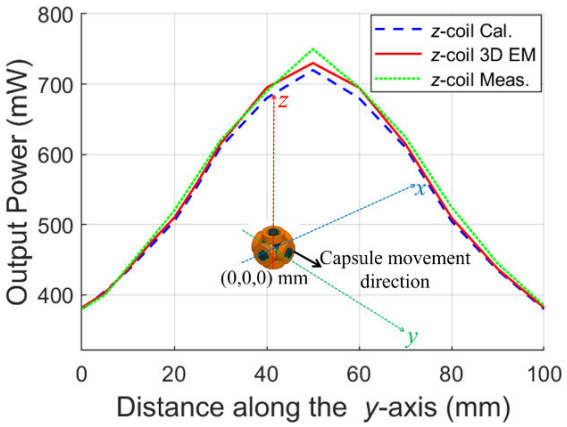

FIGURE 11. Output power variation obtained by the *z*-coil with respect to distance along the *y*-axis while $x = 0$ mm and $z = 0$ mm.

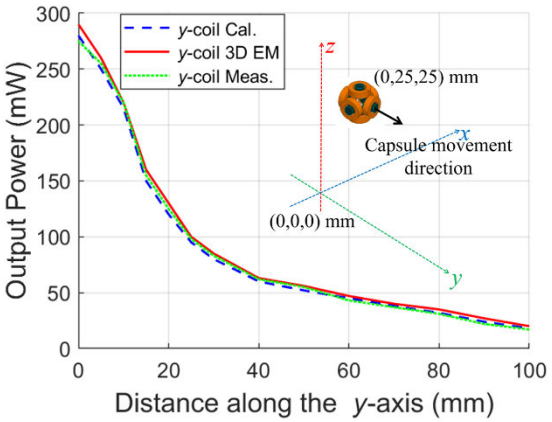

FIGURE 12. Output power variation obtained by the *y*-coil with respect to distance along the *y*-axis while $x = 25$ mm and $z = 25$ mm.

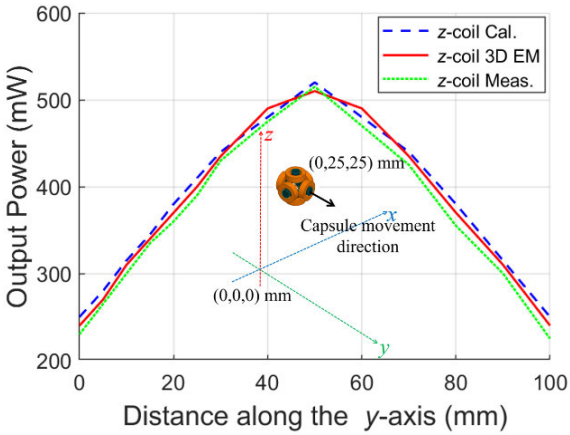

FIGURE 13. Output power variation obtained by the *z*-coil with respect to distance along the *y*-axis while $x = 25$ mm and $z = 25$ mm.

with respect to TX1 and TX2 for this experiment to reduce measurement complexity. Therefore, the received power in the x-coil is negligible. Results were taken from 0 to 100 mm distance variation in the y-axis of the 3D-RX. Maximum percentage of error on the output power between the three types of results is less than 10%. In Fig, 10, 12, and 14, the gradual reduction of output power is due to the movement of the y-coil of 3-D RX away from the center of the TX coil towards the region where the magnetic field distribution is lower. However, in Fig. 11, 13, and 15, the z-coil of 3-D RX moves from a lower magnetic field region to the higher (to the center of a TX coil) and finally again towards lower region. Therefore, the output power is initially low and it increases with the distance to a point where z-coil is near the center of the TX coil and it reduces again as the RX coil moves away from the center gradually.

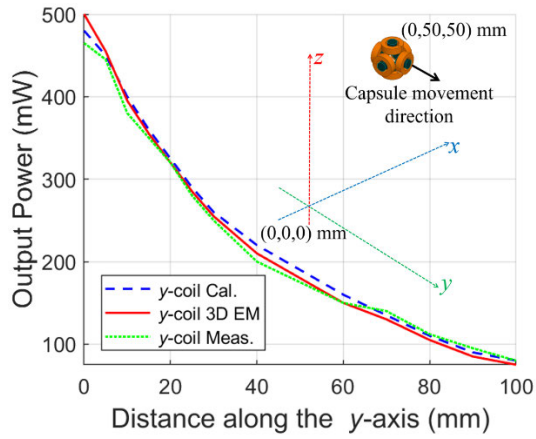

FIGURE 14. Output power variation obtained by the *y*-coil with respect to distance along the *y*-axis while $x = 50$ mm and $z = 50$ mm.

2) MEASUREMENT IN LIQUID PHANTOM

Measurements of the output power were then conducted in the liquid phantom and compared with the simulated results obtained from the EM-solver ANSYS MAXWELL 3D. The simulated result from EM-solver was taken as the reference data and stored in a look-up table. Measurements were carried out as the 3-D RX coil was moved from the start to the end position along the relevant axis. This process was repeated 5 times. The variation of powers from the measurements is due to the human error in positioning accurately

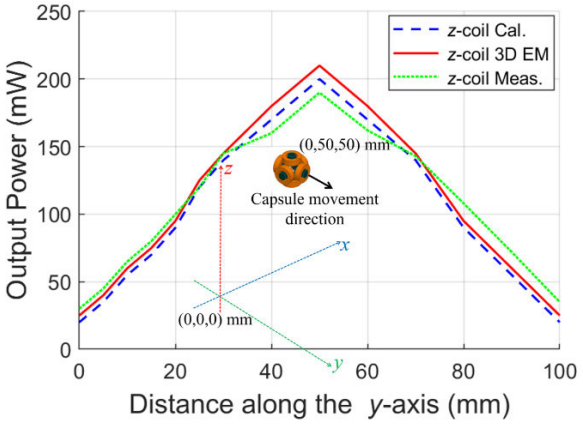

FIGURE 15. Output power variation obtained by the z-coil with respect to distance along the y-axis while $x = 50$ mm and $z = 50$ mm.

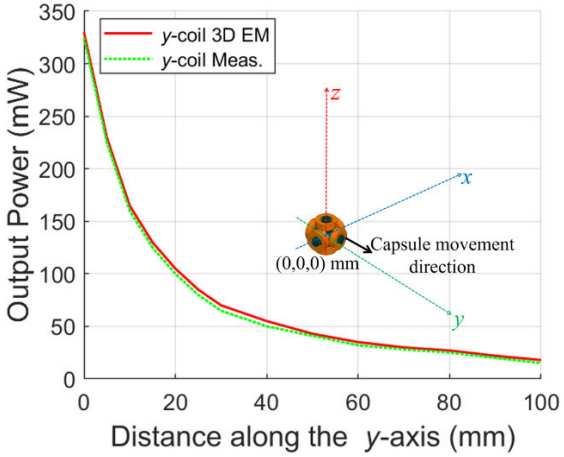

FIGURE 16. Output power variation of the y-coil as the 3D-RX is moved along the y-axis while $x = 0$ mm and $z = 0$ mm.

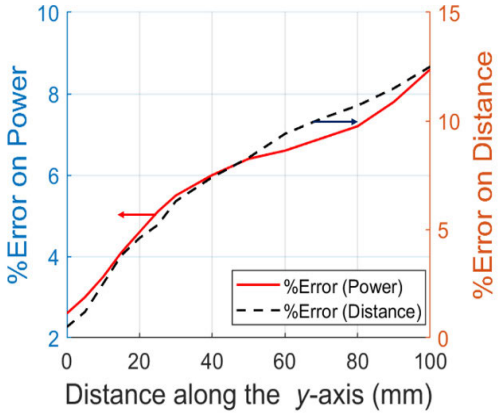

FIGURE 17. Calculated percentage of error on power of y-coil from look up table and resulting percentage of error on distance at $x = 0$ mm and $z = 0$ mm.

the 3-D RX coil holder in the phantom. The measurement data closest to the reference data was used to calculate the power and position accuracy of the proposed localization technique.

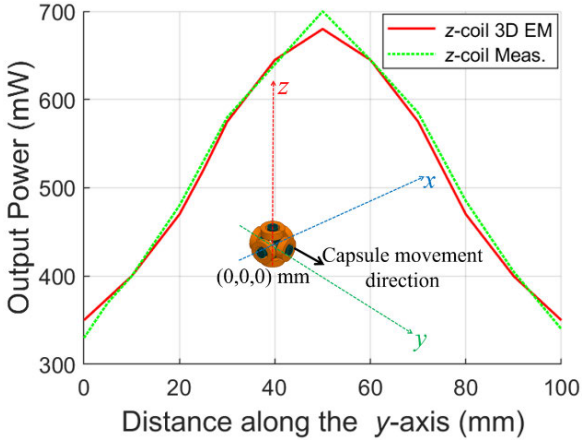

FIGURE 18. Output power variation of the z-coil as the 3D-RX is moved along the y-axis at y-axis while $x = 0$ mm and $z = 0$ mm.

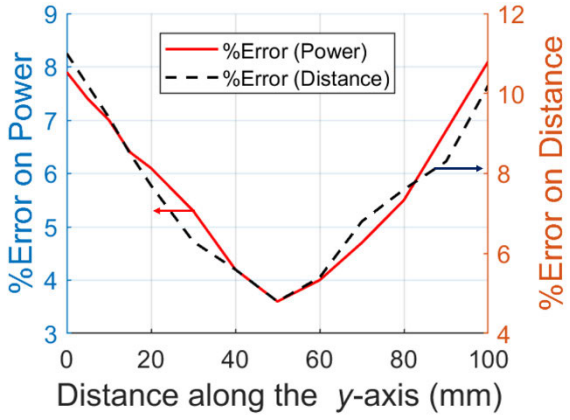

FIGURE 19. Calculated percentage of error on power of z-coil from look up table and resulting percentage of error on distance at $x = 0$ mm and $z = 0$ mm.

Figure 16 shows the variation of the output power for the y-coil as the perfectly aligned 3-D RX is moved along the y-axis with x- and z-positions kept at 0 mm. In this case, Fig. 17 shows that the maximum percentage of error on the output power (red solid curve) is close to 9% at 10 cm translational misalignment of 3-D RX with respect to TX2 coil. At this position, this error leads to a maximum of 12% inaccuracy in the measurement of the position of the capsule (broken black curve). This worst-case error is measured at the distance where the received power is significantly low. Such a distance is usually outside the boundary of the GI tract for an average human body. A similar measurement of the z-coil of the 3-D RX is shown in Fig. 18 where errors of less than 4% and 8% on the output power are measured at 5 cm and 10 cm translational distance, respectively, along the y-axis for TX1 coil, as shown in Fig. 19. The percentage of error on the power translates to a percentage of error of 5% and 10% at 5 cm and 10 cm distance, respectively, along the y-axis.

Further measurements for $x = 10$ mm, $x = 25$ mm and $x = 50$ mm (not presented here) were conducted for

TABLE 2. Record of measurement of %error on power and distance for different locations of 3-D RX coil inside the liquid phantom.

Peak power (mW) (*y*-position, cm)	Worst case percentage of error on output power (%)	Worst case percentage of error on distance (%)	Relevant distance along y-axis (cm)	Comments
x = 10 mm & z = 0 mm				
305 (0)	9	11	10	*y*-coil
680 (50)	8.5	9	10	z-coil
x = 25 mm & z = 0 mm				
265 (0)	10	13	10	*y*-coil
635 (50)	8	9.5	0	*z*-coil
x = 50 mm & z = 0 mm				
140 (0)	7.8	12	10	*y*-coil
410 (50)	9	7	10	*z*-coil
x = 0 mm & z = 50 mm				
585 (0)	8	10.5	10	*y*-coil
315 (50)	7	8.5	0	*z*-coil
x = 25 mm & z = 25 mm				
255 (0)	9.5	12.7	10	*y*-coil
480 (50)	9.7	8	10	*z*-coil
x = 50 mm & z = 50 mm				
435 (0)	10.5	12	10	*y*-coil
165 (50)	8.8%	13	10	*z*-coil

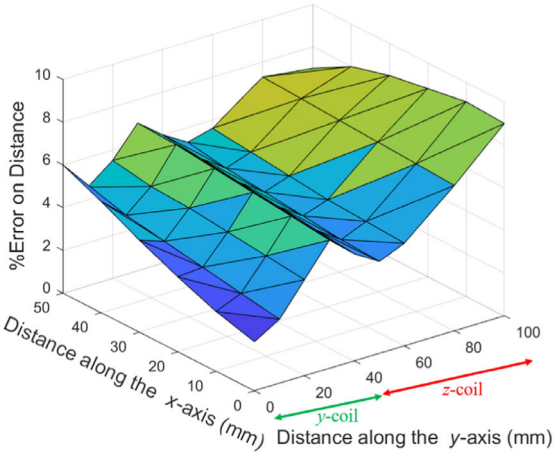

FIGURE 20. Minimum %error on distance along *y*-axis when 3-D RX is moving towards *x*-axis for $z = 0$ mm.

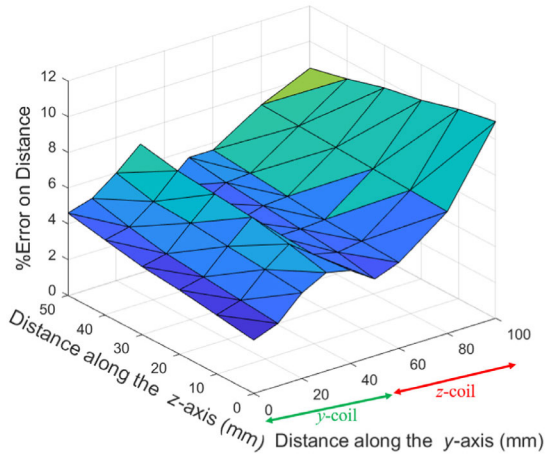

FIGURE 21. Minimum %error on distance along *y*-axis when 3-D RX is moving towards *z*-axis for $x = 0$ mm.

translation of the coil along the *y*- and *z*-axes. Similar graphs as those obtained for $x = 0$ mm can be drawn for the *y*-coil and *z*-coil. Table 2 provides peak power achieved and relevant distance along the y-axis where such a peak power is achieved. The table also presents the worst-case errors on the output power, the relevant percentages of error on the distance, and the distances along the y-axis as to where these worst-case scenarios occur. The last column indicates for which coil the worst-case error occurs. A gradual degradation of output power for *y*-coil and *z*-coil is noticeable from Table 2 as the 3-D RX coil moves from $x = 0$ mm to 50 mm.

The ability to calculate independently the percentage of error in the distance using the *y*-coil and *z*-coil allows to choose the minimum percentage of error between the two coils to reduce inaccuracy in the position of the 3-D RX coil. Figure 20 shows the minimum %error on distance measured in 3-D RX coil for different distances along the *x*-axis while moving along *y*-axis keeping *z*-axis constant. A similar Fig. 21 shows the minimum %error on distance for *z*-axis while moving along *y*-axis and keeping $x = 0$ mm. In both cases, the measurement of the power in the *y*-coil provides the smallest error along the y-axis for distance up to 55 mm, followed by measurement of the power in the *z*-coil.

3) ESTIMATION OF THE TRAJECTORY OF THE CAPSULE

In real-life situations, it is not possible to visually assess the location of the capsule inside the GI tract unless continuous real-time MRI or X-ray scanning is performed; a method which limits the usefulness of capsule endoscopy. The question remains as to whether, from the sheer measurements of the powers recorded by the three 3D-RX coils, it is possible to infer the location of the capsule. This type of inverse problem is studied in this section.

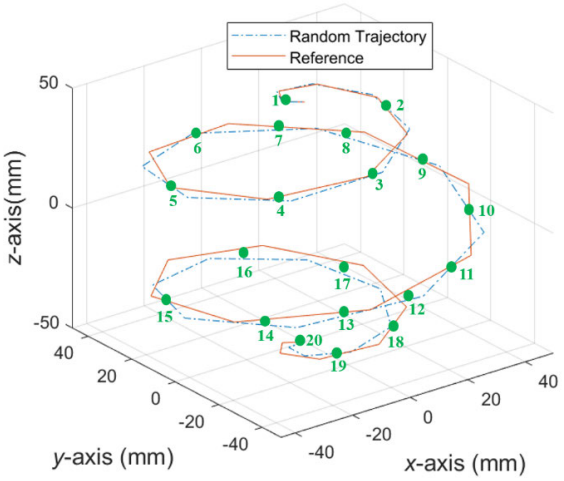

FIGURE 22. Blind trajectory estimation and comparison with reference in 100 × 100 × 100 mm^3 space inside the phantom.

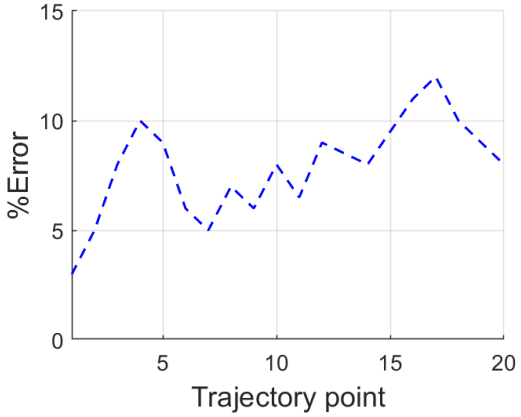

FIGURE 23. Percentage of error in the distance data with the blind trajectory.

TABLE 3. Comparison of different localization techniques.

Ref	Technique	Frequency (MHz)	Measurement Medium	Worst Error (mm)	SAR (W/kg)
[34]	DOA and TOA	-	10 cm×10 cm×50 cm (Simulation)	10	-
[35]	RSS	-	32 cm×32 cm×26.8 cm	50	-
[36]	RSS and TOA	900	Human model: simulation and real	50	-
This work	WPT	5	10 cm ×10 cm×10 cm (Phantom)	±13	0.55

In this section, the measured input power data are used to estimate the trajectory of the 3-D RX coil within the phantom and compare it with reference data. As shown in Fig. 22, this trajectory describes a hypothetical downward journey (z decreasing) of an endoscopic capsule inside the GI tract. Although the anatomical configuration of the GI tract is more complex than a helix, the trajectory provides the essential features needed in terms of potential movement of the coil in the 3 directions. Values of the output power in the three 3-D RX coil were simulated and stored as reference data as the capsule was following a random trajectory in the phantom. The simulated data is collected from EM-solver ANSYS MAXWELL 3D. Figure 22 shows the measured trajectory path (labelled random trajectory) compared with the obtained simulated values from the look-up table (labelled reference) of the 3-D RX coil in a 100 × 100 × 100 mm^3 space inside the phantom.

It is challenging to calculate the percentage of error on the distance across the 3 dimensions for the random trajectory of the 3-D RX coil compared with the reference trajectory. Therefore, a simpler approach was adopted by selecting 20 trajectory points (shows as green dots) in Fig. 22. Figure 23 calculates the percentage of error in distance of the simulated data with respect to the random trajectory at the trajectory points represented by the green dots. The percentage of error is calculated by taking the minimum percentage of error obtained by the 3 coils and compares it with the blind trajectory. The maximum percentage of error is 12% which leads to a ±13 mm of distance offset with respect to the reference data.

Most of the techniques for localization techniques used in the literature are based on simulation and measurements in phantom or human body are rare. Table 3 provides a general comparison of the proposed localization technique with previously published works [34]–[36]. In [34], the worst error is 10 mm. However, this technique is solely based on simulation results. In [36], the measurement in human body is conducted in air where the measurement antennas are located at body surface. In most of the previous research, tissue safety in terms of SAR is not provided as an evaluation parameter. However, it is important to verify the SAR as most of these techniques require higher operating frequency which increases the SAR. The proposed technique is simulated and also verified experimentally in a liquid phantom. Furthermore, the SAR is also simulated to verify that tissue safety guidelines are being complied to.

V. CONCLUSION AND FUTURE WORK

The potential of WPT technique for capsule location identification has been studied and investigated in this article. Agar-based liquid phantom has been prepared and tested at lower frequency for the validation of the proposed technique.

The measurements were conducted both in air and phantom inside a human shaped mannequin which is rare in the literature. The cross-type 3-D RX coil is used to conduct the location measurement. Two orthogonally positioned TX coils are used to create a 3-D magnetic field space which is represented with the received power into a 3-D matrix look-up table. The received power data indicates the corresponding

location of the 3-D RX coil therefore of the capsule. The reference data in the look-up table is used to find the trajectory of the 3-D RX coil used in this experiment. In this work, five data sets are used to verify the performance of this proposed CE localization technique and compared to the EM solver data set used as reference. The measurement results show that, in the acceptable range of translational misalignment of the 3-D RX coil in any axis, the worst-case error on distance due to error on measured output power is approximately 6% achievable compared with the reference data. The trajectory experiment demonstrates a percentage of error on distance of approximately 12% during the measurement on a 100 mm×100mm×100mm volume filled with the liquid phantom. The blind trajectory experiments could provide lower translational misalignment of the 3-D RX if the number of TX coils were to be increased. Also the development of custom built application specific IC (ASIC) including power processing and ADC unit is in consideration to accommodate the 3-D RX and necessary circuitry within the space of the capsule.

In conclusion, the measurement results presented in this paper show a promising WPT-based localization technique for capsule endoscopy and other implantable medical devices.

REFERENCES

[1] H. Mateen, R. Basar, A. U. Ahmed, and M. Y. Ahmad, "Localization of wireless capsule endoscope: A systematic review," *IEEE Sensors J.*, vol. 17, no. 5, pp. 1197–1206, Mar. 2017, doi: 10.1109/JSEN.2016.2645945.

[2] I. Umay, B. Fidan, and B. Barshan, "Localization and tracking of implantable biomedical sensors," *Sensors*, vol. 17, no. 3, p. 583, 2017, doi: 10.3390/s17030583.

[3] T. D. Than, G. Alici, H. Zhou, and W. Li, "A review of localization systems for robotic endoscopic capsules," *IEEE Trans. Biomed. Eng.*, vol. 59, no. 9, pp. 2387–2399, Sep. 2012, doi: 10.1109/TBME.2012.2201715.

[4] G. Ciuti, A. Menciassi, and P. Dario, "Capsule endoscopy: From current achievements to open challenges," *IEEE Rev. Biomed. Eng.*, vol. 4, pp. 59–72, 2011, doi: 10.1109/RBME.2011.2171182.

[5] K. Duda, T. Zielinski, R. Fraczek, J. Bulat, and M. Duplaga, "Localization of endoscopic capsule in the GI tract based on MPEG-7 visual descriptors," in *Proc. IEEE Int. Workshop Imag. Syst. Techn.*, May 2007, pp. 1–4, doi: 10.1109/ist.2007.379580.

[6] J. Bulat, K. Duda, M. Duplaga, R. Fraczek, A. Skalski, M. Socha, P. Turcza, and T. P. Zelinski, "Data processing tasks in wireless GI endoscopy: Image-based capsule localization & navigation and video compression," in *Proc. Annu. Int. Conf. IEEE Eng. Med. Biol.*, Aug. 2007, pp. 2815–2818, doi: 10.1109/IEMBS.2007.4352914.

[7] H. Lay, G. Cummins, B. F. Cox, Y. Qin, M. V. Turcanu, R. McPhilips, C. Connor, R. Gerson, E. Clutton, M. P. Y. Desmulliez, and S. Cochran, "*In-vivo* evaluation of microultrasound and thermometric capsule endoscopes," *IEEE Trans. Biomed. Eng.*, vol. 66, no. 3, pp. 632–639, Mar. 2019, doi: 10.1109/TBME.2018.2852715.

[8] F. Carpi, N. Kastelein, M. Talcott, and C. Pappone, "Magnetically controllable gastrointestinal steering of video capsules," *IEEE Trans. Biomed. Eng.*, vol. 58, no. 2, pp. 231–234, Feb. 2011, doi: 10.1109/TBME.2010.2087332.

[9] I. Wilding, P. Hirst, and A. Connor, "Development of a new engineering-based capsule for human drug absorption studies," *Pharmaceutical Sci. Technol. Today*, vol. 3, no. 11, pp. 385–392, 2000, doi: 10.1016/S1461-5347(00)00311-4.

[10] T. D. Than, G. Alici, H. Zhou, S. Harvey, and W. Li, "Enhanced localization of robotic capsule endoscopes using positron emission markers and rigid-body transformation," *IEEE Trans. Syst., Man, Cybern. Syst.*, vol. 49, no. 6, pp. 1270–1284, Jun. 2019, doi: 10.1109/TSMC.2017.2719050.

[11] M. Pourhomayoun, Z. Jin, and M. L. Fowler, "Accurate localization of in-body medical implants based on spatial sparsity," *IEEE Trans. Biomed. Eng.*, vol. 61, no. 2, pp. 590–597, Feb. 2014, doi: 10.1109/TBME.2013.2284271.

[12] D. Fischer, R. Schreiber, D. Levi, and R. Eliakim, "Capsule endoscopy: The localization system," *Gastrointestinal Endoscopy Clin. North Amer.*, vol. 14, no. 1, pp. 25–31, 2004, doi: 10.1016/J.GIEC.2003.10.020.

[13] B. Fidan and I. Umay, "Adaptive environmental source localization and tracking with unknown permittivity and path loss coefficients," *Sensors*, vol. 15, no. 12, pp. 31125–31141, Dec. 2015, doi: 10.3390/s151229852.

[14] T. Shah, S. M. Aziz, and T. Vaithianathan, "Development of a tracking algorithm for an *in-vivo* RF capsule prototype," *Proc. 4th Int. Conf. Electr. Comput. Eng. (ICECE)*, Dec. 2006, pp. 173–176, doi: 10.1109/ICECE.2006.355318.

[15] L. Wang, L. Liu, C. Hu, and M. Q.-H. Meng, "A novel RF-based propagation model with tissue absorption for location of the GI tract," in *Proc. Annu. Int. Conf. IEEE Eng. Med. Biol. Soc.*, Sep. 2010, pp. 654–657, doi: 10.1109/IEMBS.2010.5627228.

[16] L. Wang, C. Hu, L. Tian, M. Li, and M. Q.-H. Meng, "A novel radio propagation radiation model for location of the capsule in GI tract," in *Proc. IEEE Int. Conf. Robot. Biomimetics (ROBIO)*, Dec. 2009, pp. 2332–2337, doi: 10.1109/ROBIO.2009.5420456.

[17] K. Arshak and F. Adepoju, "Adaptive linearized methods for tracking a moving telemetry capsule," in *Proc. IEEE Int. Symp. Ind. Electron.*, Jun. 2007, pp. 2703–2708, doi: 10.1109/ISIE.2007.4375035.

[18] R. Chandra, A. J. Johansson, and F. Tufvesson, "Localization of an RF source inside the human body for wireless capsule endoscopy," in *Proc. 8th Int. Conf. Body Area Netw.*, 2013, pp. 48–54, doi: 10.4108/icst.bodynets.2013.253713.

[19] C. Hekimian-Williams, B. Grant, X. Liu, Z. Zhang, and P. Kumar, "Accurate localization of RFID tags using phase difference," in *Proc. IEEE Int. Conf. RFID*, Apr. 2010, pp. 89–96, doi: 10.1109/RFID.2010.5467268.

[20] Le Zhang, Y. Zhu, T. Mo, J. Hou, and H. Hu, "Design of 3D positioning algorithm based on RFID receiver array for *In vivo* micro-robot," in *Proc. 8th IEEE Int. Conf. Dependable, Auton. Secure Comput.*, Dec. 2009, pp. 749–753, doi: 10.1109/DASC.2009.95.

[21] A. Wille, M. Broll, and S. Winter, "Phase difference based RFID navigation for medical applications," in *Proc. IEEE Int. Conf. RFID*, Apr. 2011, pp. 98–105, doi: 10.1109/RFID.2011.5764608.

[22] S. R. Khan, S. K. Pavuluri, G. Cummins, and M. P. Y. Desmulliez, "Miniaturized 3-D cross-type receiver for wirelessly powered capsule endoscopy," *IEEE Trans. Microw. Theory Techn.*, vol. 56, no. 5, pp. 1985–1993, May 2019, doi: 10.1109/TMTT.2019.2893204.

[23] S. R. Khan, S. K. Pavuluri, and M. P. Y. Desmulliez, "Accurate modeling of coil inductance for near-field wireless power transfer," *IEEE Trans. Microw. Theory Techn.*, vol. 66, no. 9, pp. 4158–4169, Sep. 2018, doi: 10.1109/TMTT.2018.2854190.

[24] P. T. Theilmann and P. M. Asbeck, "An analytical model for inductively coupled implantable biomedical devices with ferrite rods," *IEEE Trans. Biomed. Circuits Syst.*, vol. 3, no. 1, pp. 43–52, Feb. 2009, doi: 10.1109/TBCAS.2008.2004776.

[25] A. Karalis, J. D. Joannopoulos, and M. Soljačić, "Efficient wireless non-radiative mid-range energy transfer," *Ann. Phys.*, vol. 323, no. 1, pp. 34–48, 2008, doi: 10.1016/j.aop.2007.04.017.

[26] C. Moorey, W. Holderbaum, and B. Potter, "Investigation of high-efficiency wireless power transfer criteria of resonantly-coupled loops and dipoles through analysis of the figure of merit," *Energies*, vol. 8, no. 10, pp. 11342–11362, Sep. 2015, doi: 10.3390/en81011342.

[27] A. Kurs, A. Karalis, R. Moffatt, J. D. Joannopoulos, P. Fisher, and M. Soljačić, "Wireless power transfer via strongly coupled magnetic resonances," *Science*, vol. 317, no. 5834, pp. 83–86, 2007, doi: 10.1126/science.1143254.

[28] S. R. Khan and G. S. Choi, "Analysis and optimization of four-coil planar magnetically coupled printed spiral resonators," *Sensors*, vol. 16, no. 8, p. 1219, 2016, doi: 10.3390/s16081219.

[29] M. Kiani, U.-M. Jow, and M. Ghovanloo, "Design and optimization of a 3-coil inductive link for efficient wireless power transmission," *IEEE Trans. Biomed. Circuits Syst.*, vol. 5, no. 6, pp. 579–591, Dec. 2011, doi: 10.1109/Tbcas.2011.2158431.

[30] M. Kiani and M. Ghovanloo, "A figure-of-merit for designing high-performance inductive power transmission links," *IEEE Trans. Ind. Electron.*, vol. 60, no. 11, pp. 5292–5305, Nov. 2013, doi: 10.1109/TIE.2012.2227914.

[31] K. N. Bocan, M. H. Mickle, and E. Sejdić, "Multi-disciplinary challenges in tissue modeling for wireless electromagnetic powering: A review," *IEEE Sensors J.*, vol. 17, no. 20, pp. 6498–6509, Oct. 2017, doi: 10.1109/JSEN.2017.2748338.

[32] T. Yamamoto, K. Sano, K. Koshiji, X. Chen, S. Yang, M. Abe, and A. Fukuda, "Development of electromagnetic phantom at low-frequency band," in *Proc. Annu. Int. Conf. IEEE Eng. Med. Biol. Soc. (EMBS)*, Jul. 2013, pp. 1887–1890, doi: 10.1109/EMBC.2013.6609893.

[33] IT'IS Foundation. *Tissue Frequency Chart*. Accessed: Feb. 27, 2019. [Online]. Available: https://itis.swiss/virtual-population/tissue-properties/database/tissue-frequency-chart/

[34] A. Nafchi, S. T. Goh, and S. R. Zekavat, "Circular arrays and inertial measurement unit for DOA/TOA/TDOA-based endoscopy capsule localization: Performance and complexity investigation," *IEEE Sensors J.*, vol. 14, no. 11, pp. 3791–3799, Nov. 2014, doi: 10.1109/JSEN.2014.2331244.

[35] Y. Ye, P. Swar, K. Pahlavan, and K. Ghaboosi, "Accuracy of RSS-based RF localization in multi-capsule endoscopy," *Int. J. Wireless Inf. Netw.*, vol. 19, no. 3, pp. 229–238, Sep. 2012, doi: 10.1007/s10776-012-0193-1.

[36] U. Khan, Y. Ye, A.-U. Aisha, P. Swar, and K. Pahlavan, "Precision of EM simulation based wireless location estimation in multi-sensor capsule endoscopy," *IEEE J. Transl. Eng. Health Med.*, vol. 6, pp. 1–11, 2018, doi: 10.1109/JTEHM.2018.2818177.

SADEQUE REZA KHAN received the B.Sc. degree in electronics and telecommunication engineering from the University of Liberal Arts Bangladesh, in 2010, the M.Tech. degree in VLSI design from the National Institute of Technology Karnataka, India, in 2014, and the Ph.D. degree in electrical engineering from Heriot-Watt University, U.K. He is currently working as a Postdoctoral Researcher with the Institute for Integrated Micro and Nano Systems, The University of Edinburgh, U.K. His research interests include embedded systems, ASIC, and wireless power transfer.

SRINJOY MITRA (Senior Member, IEEE) received the M.Tech. degree from the Indian Institute of Technology, Bombay, India, and the Ph.D. degree from the Institute of Neuroinformatics (UNI), ETH Zurich, Switzerland. He was a Postdoctoral Researcher with Johns Hopkins University, Baltimore, MD, USA, before joining the Medical Electronics Team, IMEC, Belgium. He is currently a Senior Lecturer with the Institute for Integrated Micro and Nano Systems, The University of Edinburgh, U.K. His primary research interests include mixed-signal circuits and systems for sensor interfaces.

MARC P. Y. DESMULLIEZ (Senior Member, IEEE) received the degrees (five) in microwave engineering, optoelectronics, and theoretical physics from University College London, the University of Cambridge, and Heriot-Watt University. He currently manages the Medical Device Manufacturing Centre (www.mdmc.hw.ac.uk), Heriot-Watt University, where he holds the position of the Deputy Head of the Research Institute in Signals, Sensors and Systems. He is the Acting CEO of the company Microsense Technologies Ltd., (www.microsensetechnologies.com). He has coauthored around 500 peer-reviewed publications and holds nine patents. He was recently awarded the Recipient of the National Instruments Global Engineering Impact Prize, in 2019, for his work on capsule endoscopy.